ARTICLE

OBC
www.rsc.org/obc

The four-electron diamagnetic ring current of porphycene

Erich Steiner and Patrick W. Fowler*
School of Chemistry, University of Exeter, Stocker Road, Exeter, UK EX4 4QD.
E-mail: P.W.Fowler@exeter.ac.uk; Fax: +44 1392 263434

Received 14th October 2002, Accepted 12th March 2003
First published as an Advance Article on the web 10th April 2003

Porphycene, an isomer that can replace porphin in chemical and biochemical contexts, is predicted by *ab initio* calculation to exhibit a global diatropic π ring current with bifurcation across the four pyrrole units of the macrocycle. Analysis of the orbital contributions to the current density in porphycene reveals that the global current, with its bifurcation feature, is attributable to the four electrons of the near-degenerate HOMO levels, the same set of active electrons that feature in the well-known four-orbital model of the electronic spectra of porphyrins. Integration of the current density gives ^{1}H, ^{13}C and ^{15}N NMR shieldings that are compatible with the observed low-field shifts of peripheral and bridge protons and high-field shift of the internal NH protons, assignment of the ^{13}C NMR spectrum and the single average ^{15}N chemical shift resulting from rapid NH tautomerism. Geometries were calculated with the DFT B3LYP functional, the current density maps were calculated with the ipsocentric coupled-Hartree–Fock CTOCD-DZ method, and the shieldings with the CTOCD-PZ2 variant, all in the same 6-31G** basis.

1. Introduction

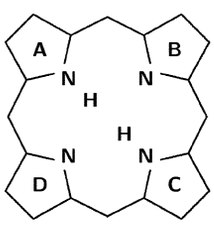

1

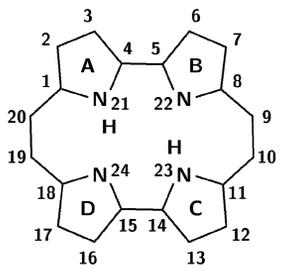

2

Porphycene, **2**, an isomer of porphin, **1**, was first reported in 1986 by Vogel and co-workers,[1] the authors of the report expressing surprise that this porphyrin-like compound should have avoided detection for so long. Porphycene has many of the chemical and physical properties that are characteristic of the family of aromatic porphyrins,[1] including planarity of the macrocycle, ^{1}H NMR with NH protons at very high field and CH protons at low field, colour, with main absorption bands having high molar absorption coefficient, and an intense double Soret band. Indeed, calculations have suggested that porphycene and porphin have almost identical energies, with some doubt as to which is in fact lower.[2] Porphycene has been discussed as a photo-sensitiser for photo-dynamic therapy,[3] and its substitution for porphin can provide insights into structure–function relationships in biology, as in the recent demonstration of a high oxygen affinity for a blue myoglobin reconstituted with an iron porphycene.[4] The similarities observed between porphycene and porphin suggest that the same structural factors and theoretical principles apply to both. In particular, the explanation of the principal bands of the electronic spectrum in terms of $\pi \longrightarrow \pi^*$ transitions within a 'four-orbital' model[5] should apply, involving combinations of one-electron transitions from the two highest occupied (HOMO and HOMO − 1) to the two lowest unoccupied molecular orbitals (LUMO and LUMO + 1).

We have shown that, within the ipsocentric orbital model of current density,[6,7] the same transitions as those in the four-orbital model of electronic spectra explain the characteristically aromatic π ring currents in porphin, chlorin and bacteriochlorin.[8,9] These systems obey the 4-electron rule for closed-shell monocyclic ring systems, whereby the π current density is dominated by contributions from the translationally-allowed transitions from the HOMO pair to the LUMO pair. Thus, in common with other physical and chemical properties that distinguish the whole molecule from its parts, the global response of a molecule to an external magnetic field is a property of its most mobile electrons: those with the most ready access to excited states.

It is demonstrated in the present work by direct mapping of the induced current density that the π ring current of porphycene also displays the 4-electron bifurcated global circulation that is characteristic of the family. Whilst the conventional interpretation of diatropic/paratropic (aromatic/antiaromatic) behaviour in terms of NICS values[10,11] gives a misleading picture of the local flow of current in the two types of pyrrole ring (with and without NH bond), the local patterns of current density are readily interpreted in terms of the details of the bifurcated flow across the pyrrole rings. Computed nuclear shieldings are consistent with experimental ^{1}H, ^{13}C and ^{15}N values, and they demonstrate the overall correctness of the present description of the magnetic properties of the system.

Porphycene is thus magnetically, as well as structurally, chemically and biochemically, a close model of porphin, in that it possesses a macrocyclic ring current related to its frontier-orbital electronic structure, a feature that may be significant in view of the growing importance of ring-current related chemical shifts in solid-state NMR as a tool for structural assignment in supramolecular systems.[12]

2. Geometry

The ground-state geometry of porphycene used here to present the magnetic properties was computed within density functional theory (DFT) with the B3LYP functional and 6-31G** basis set, as implemented in Gaussian98.[13] This is a move away from our previous use of RHF (restricted Hartree–Fock) theory, with the same basis, and has been made necessary by the lower reliability of RHF geometries for larger flexible ring structures. The ground state of porphycene in DFT has the *trans* C_{2h} geometry **2**,[14] and the 6-31G** geometric parameters differ only little from the values listed by Kozlowski *et al.* for the basis sets 6-31G* and TZ2P. They are also similar to the optimum values obtained for the C_{2h} structure at the RHF/6-31G** level, but this is *not* a minimum on the RHF surface, as relaxation of the structure gives a distorted planar (C_s)

DOI: 10.1039/b210115g

Table 1 Geometric parameters for porphycene, calculated at three levels of theory within the 6-31G** basis: DFT denotes full optimisation using the B3LYP functional; RHF (C_{2h}) denotes symmetry-constrained optimisation at the RHF level; RHF (C_s) denotes full optimisation at the RHF level, as discussed in the text

Bond type		Bond lengths (Å)		
		DFT (C_{2h})	RHF (C_{2h})	RHF (C_s)
CN		1.36 ± 0.01	1.34 ± 0.01	1.30 ⟶ 1.38
CC	Link and bridge	1.39, 1.41	1.38, 1.40	1.35 ⟶ 1.45
	Peripheral	1.37, 1.38	1.35, 1.36	1.34 ⟶ 1.40
	Shoulder	1.43 ⟶ 1.46	1.42 ⟶ 1.45	1.39 ⟶ 1.46

structure, which lies only 12 kJ mol^{-1} lower in energy, but has a quite different pattern of bond lengths.

The geometric parameters for the three calculations are summarised in Table 1. In C_{2h} symmetry, DFT and RHF give identical patterns of longer and shorter bonds, with RHF values in general smaller than DFT values by up to 0.025 Å for CN bonds, 0.02 Å for CC bonds in the local rings, 0.01 Å for links and bridges. The four pyrrole-type rings are very similar to each other, with computed bond lengths that are insensitive to N protonation. The bridges show almost no bond alternation. In contrast, the distorted optimum C_s RHF geometry shows substantial, and unpredictable, variations in bond lengths, all four rings are different, and the two bridges have different patterns of bond alternation.

Similar difficulties arise for porphin (**1**) itself.[15] In this case, DFT gives the expected D_{2h} symmetry with geometric parameters similar to the RHF values in D_{2h}. The symmetry-broken optimum C_{2v} RHF geometry of porphin, however, shows strong variation in bond lengths as found in the symmetry-broken optimum C_s RHF geometry of porphycene.

The essential conclusions of our geometric studies at the two levels of theory have been confirmed by corresponding studies of a range of molecules (for example, benzene, pyrrole, naphthalene, coronene) for which magnetic properties have been presented in previous work. In all cases, when computed in the same symmetry, RHF bond lengths are systematically shorter than DFT values by up to about 0.03 Å. These small differences appear to have little influence on the computed magnetic properties discussed here, as will be demonstrated for porphycene.

3. Magnetic properties

Magnetic properties were computed by the coupled Hartree–Fock method using distributed-origin methods with the Exeter version of SYSMO.[16] For the current-density maps, the diamagnetic-zero (DZ) variant of the continuous transformation of origin of current density (CTOCD) method was used,[17–21] with current density at each point in the molecule computed ipsocentrically, *i.e.* choosing the point itself as the origin of vector potential (gauge origin). This approach has been found to give satisfactory current density maps with the 6-31G** basis set used here.[19] The integrated properties (magnetisability, absolute shieldings at nuclei and at centres of rings) were computed using the paramagnetic-zero variant (PZ2) of CTOCD.[20]

Current density maps

The maps in Fig. 1 show the current density induced by a magnetic field acting at right angles to the plane of the nuclei, and are plotted in the plane at 1 a_0 above that of the nuclei. As in previous work, this choice is governed by a number of factors. This plane is close to the maximum of π current and electron density. At this height the computed maps are insensitive to an increase in basis set size beyond that of the 6-31G** set used here.[19] Also at this height, there is relatively little contamination from induced current density parallel to the external field,[22] so that the displayed current density, showing in-plane projections of current, is a good representation of the total.[23] In the plots, diamagnetic circulation is shown as anticlockwise, paramagnetic as clockwise. Maps are plotted for the total current density for all the electrons, the contribution of the π electrons, and separate contributions from selected orbitals, using the ipsocentric orbital decomposition.[6]

As expected from the close relationship of porphycene and porphin, the total π current (shown in Fig. 1e) is dominated by the contributions of the four electrons in the highest lying occupied orbitals, $6a_u$ (Fig. 1a) and $7a_u$ (Fig. 1b). In atomic units (1 au = $e\hbar/m_e a_0^4$) the total π current density in benzene (in the 1 a_0 plane, with the same basis and method) has maximum value 0.078. The corresponding maximum of total π current density in the present case is 0.162, made up of contributions 0.094 from the two electrons in the $7a_u$ HOMO, 0.084 from the two in the $6a_u$ HOMO − 1, giving net 0.159 (Fig. 1c), and 0.035 from the remaining 24 π electrons (Fig. 1d). These are the current density values for the optimum DFT geometry. Closely similar values are obtained at the C_{2h} RHF geometry (0.164 for total π, 0.095 for $7a_u$, 0.085 for $6a_u$, 0.035 for the remainder), but *not* at the optimum C_s RHF geometry in which the large variations of bond length are accompanied by much reduced π current density (*e.g.* 0.087 for total π).

In Fig. 2 is shown the relevant part of the orbital energy level diagram, from which the main virtual transitions responsible for the induced current density can be identified, and the sense of circulation of the induced currents deduced. The diagrams for the two C_{2h} geometries are essentially identical; the symmetry-broken RHF optimum C_s geometry gives a larger HOMO–LUMO gap and, of course, different symmetry labels, but the correspondence of molecular orbitals remains clear. In C_{2h} symmetry, selection rules for π orbital transitions in the presence of the perpendicular magnetic field are $a_u \leftrightarrow b_g$ for translational (and dipole moment) transitions, and $a_u \leftrightarrow a_u$ and $b_g \leftrightarrow b_g$ for rotational (and magnetic dipole) transitions. The transitions shown in Fig. 2, from near-degenerate HOMO and HOMO − 1 to low-lying unoccupied orbitals, are translationally allowed (in C_{2h} symmetry) and therefore give rise to global diamagnetic circulation.[6,7] The corresponding rotational transitions, to $8a_u$ (at 0.14 E_h), are less important, being at higher energy and involving mismatch of the orbital patterns of nodes. There is a group of five occupied orbitals at 0.1 to 0.13 E_h (250 to 350 kJ mol^{-1}) below the HOMO − 1 and these are mainly responsible for the 'remainder' contribution of Fig. 1d. In C_s, all the π orbitals have a″ symmetry so that all π to π* transitions become both rotationally and translationally allowed, and some blurring of the distinction between diamagnetic and paramagnetic response is to be expected. In practice however, the orbitals themselves remain similar to their C_{2h} counterparts and the predictions based on higher symmetry remain good first approximations.

A notable feature of the current density maps is the *bifurcation* of the global current around the pyrrole units in the separate orbital currents of $6a_u$ and $7a_u$ (Figs. 1a and 1b) as well as in the total π current. The fact that bifurcation is visible even at the orbital level suggests that the global bifurcated pathway should be considered as a distinct *single delocalisation pathway* around the macrocycle rather than as a superposition of simpler pathways.[9,11,24]

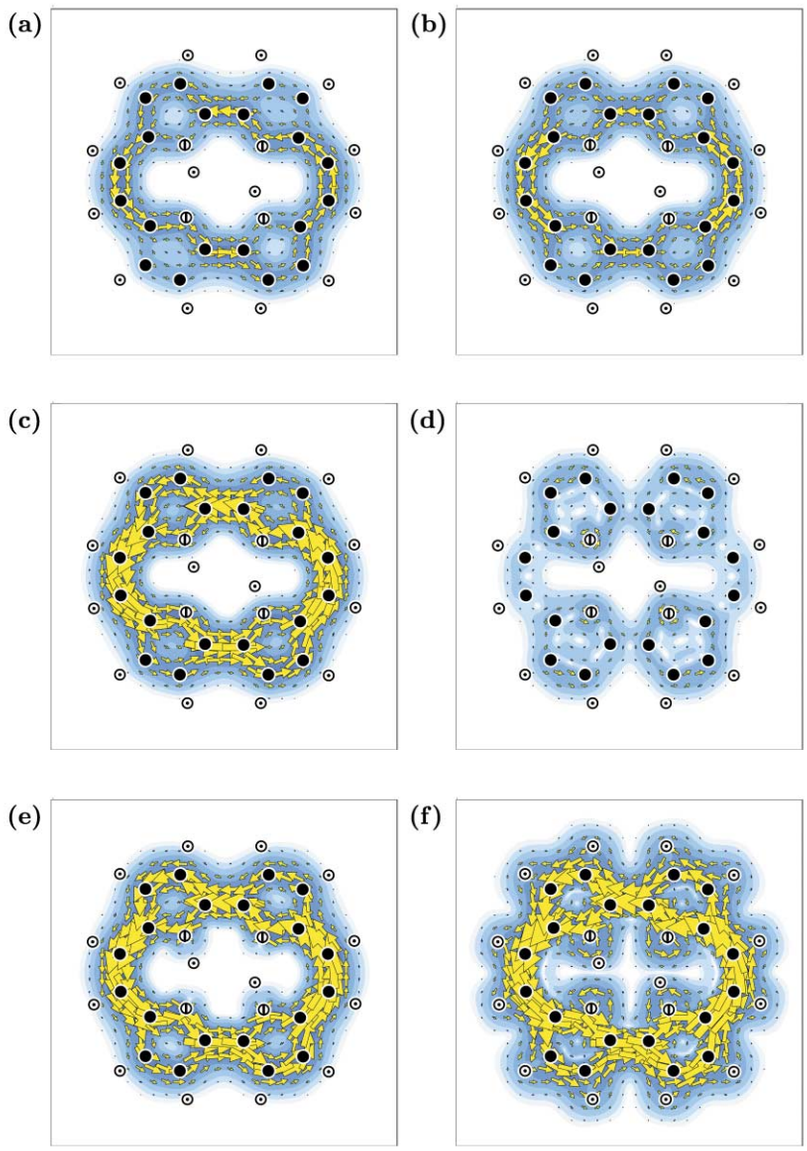

Fig. 1 Computed CTOCD-DZ current-density maps for porphycene. Contributions of (a) orbital $6a_u$, (b) orbital $7a_u$, (c) orbitals $6a_u + 7a_u$, (d) all π orbitals except $6a_u$ and $7a_u$, (e) all π orbitals, (f) all σ + π orbitals. All maps are plotted in the 1 a_0 plane as discussed in the text. Carbon, nitrogen and hydrogen positions are represented by full, barred and dotted circles, respectively.

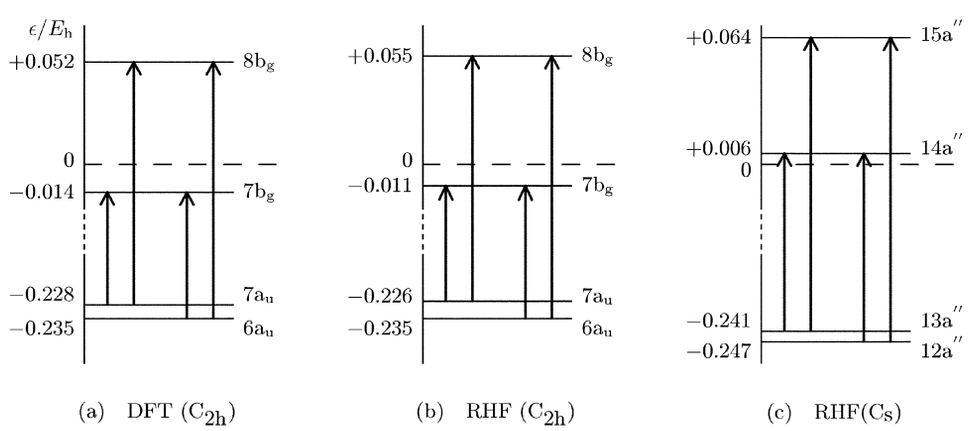

Fig. 2 Schematic orbital energy level diagrams for porphycene computed at the RHF level (6-31G** basis set) for (a) C_{2h} optimum DFT geometry, (b) C_{2h} constrained optimum RHF geometry and (c) fully optimised RHF geometry. The arrows indicate the translationally allowed transitions from occupied to unoccupied orbitals.

NICS values

A popular measure of the extent of aromaticity or anti-aromaticity to be associated with a ring of bonded atoms in a molecule is the NICS value,[10] defined as the mean absolute magnetic shielding (ppm) at the geometric centre of the ring with sign reversed. On the magnetic aromaticity scale so defined, aromatic rings have large negative NICS, implying diamagnetic (diatropic) circulation around the ring, whilst small negative and positive values imply paramagnetic

(paratropic) circulation. The standard scale, the values originally presented by Schleyer *et al.*,[10] is based on GIAO-SCF calculations with MP2/6-31G* or B3LYP/6-31G* geometries and 6-31+G* basis set. In this scheme, the benzene NICS value is −9.7 (−11.5 with the 6-31G* basis), pyracylene has value −0.1 for the 6-ring and +12.8 for the 5-ring, and pentalene has NICS value +18.1 for each 5-ring.

Variations of the basic NICS scheme have been introduced, partly to investigate the source of the ring currents (whether σ or π) and partly to avoid the difficulties associated with the use of *mean* shieldings, which necessarily mix the effects of electron circulation about an axis perpendicular to the median plane of a ring and circulations about axes within the plane. Two strategies are: computation of NICS at height 1 Å above the ring centre, NICS(1),[25] and dissection of NICS(1) into σ and π contributions.[26] A third approach has been to compute both the mean absolute shielding, σ, and the component, $\sigma_{||}$, parallel to the field (perpendicular to the plane of the ring).[27] The mean component in the molecular plane can be obtained from these, and NICS(0) is −σ. It is the out-of-plane component, $\sigma_{||}$, that is the direct, and the more sensitive, measure of the strength and direction of the average ring circulation. Positive values of $\sigma_{||}$ indicate net diamagnetic circulation (anticlockwise in the maps of Fig. 1), negative values indicate net paramagnetism. Typical values obtained with the CTOCD-PZ2 formulation of coupled Hartree–Fock theory (used for integrated properties in our work) and the 6-31G** basis set are ($-\sigma$, $\sigma_{||}$) = (−12.7, +16.3) for the diamagnetic 6-ring of benzene, (−7.2, −4.5) for the 6-ring of pyracylene and (+10.6, −56.6) for the 5-ring, and (+14.4, −66.8) for the paramagnetic 5-rings of pentalene).

The magnitudes and occasionally even the signs of NICS values depend on the details of the computation: the theoretical method, the basis set and how the geometry was obtained. Nevertheless, the NICS value scale has become a valuable and routine tool for cataloguing the types of rings found in a great variety of molecules. As a single numerical quantity, it can however give an ambiguous or misleading picture of the current density in a ring, particularly when the pattern is not that of a simple circulation. Thus, despite the differences in computation, both the above sets of NICS values agree with $\sigma_{||}$ that there is diamagnetic circulation in the 6-ring of benzene, and paramagnetic circulation in the 5-rings of pyracylene and pentalene. They agree less well for the 6-ring of pyracylene in which the current density has been shown by direct visualisation not to be a simple ring current.

In the present case, the absolute shieldings at the geometric centre of the macrocycle in porphycene are ($-\sigma$, $\sigma_{||}$) = (−15.7, +34.8), both numbers indicating global diamagnetism. The values for the two types of pyrrole ring are (−13.0, +7.6) for ring A, indicating local diamagnetism, and the values (−4.8, −11.0) for ring B suggest weak local paramagnetism. In fact, the visualisation provided by the various current density maps (Fig. 1) show that the bifurcated current density in ring A, with the protonated nitrogen, is slighter stronger on the periphery than along the inner route so that, viewed from the centre of A, the net local "circulation" is counterclockwise, apparently implying diamagnetism. The converse is true for ring B, with net local clockwise circulation, apparently implying paramagnetism. The distinction between apparent and true circulations is represented schematically in Fig. 3. Numerically, this distinction is best shown by the signs of the perpendicular component $\sigma_{||}$ (+7.6 in A, −11.0 in B), but it is a general observation that the distinction between bifurcated flow and 'real' local circulations is difficult if not impossible when only global integrated magnetic properties are calculated.

Nuclear shieldings

The computed mean nuclear shieldings of all the nuclei of porphycene are listed in Table 2. Direct comparison of the individual shieldings with experimental δ values is not possible because of rapid migration of the internal protons between the nitrogen sites which here, in contrast to porphin, is apparently not frozen out at low temperature.[14,28] The corresponding molecular sites have therefore been paired in Table 2, and the computed mean values of the pairs are used to compare with the experimental values.

Table 2 Chemical shifts in porphycene

Atom	Sites	δ^a	δ^b	Exp[c]
Hydrogen[d]	2, 7	9.85, 9.67	9.77	9.23
	3, 6	9.98, 9.87	9.93	9.67
	9,10	9.94, 10.01	9.98	9.83
	21	−1.69		~3.15
Carbon[e]	1, 8	141.8, 155.8	148.8	144.8
	2, 7	132.8, 140.8	136.8	130.5
	3, 6	128.8, 133.9	131.4	125.9
	4, 5	137.6, 148.7	143.2	135.9
	9, 10	123.4, 117.8	120.6	115.0
Nitrogen[f]	21, 22	113, 204	159	161

[a] Computed value at each site. [b] Mean computed value for each pair. [c] Observed value; Ref. 1 for ^{1}H and ^{13}C, Ref. 28 for ^{15}N. [d] Computed mean absolute shieldings for hydrogen converted to isotropic chemical shifts by $\delta(^1\text{H}) = 30.83 - \sigma(^1\text{H}) \times 10^6$ (Ref. 29). [e] Computed mean absolute shieldings for carbon converted to isotropic chemical shifts by $\delta(^{13}\text{C}) = 185.6 - \sigma(^{13}\text{C}) \times 10^6$ (Ref. 29). [f] The observed value $\delta = 161$ is a shift with respect to NH_4Cl.[28] The computed mean absolute shieldings for nitrogen have been converted to predicted δ values by the formula $\delta(^{15}\text{N}) = 217 - \sigma(^{15}\text{N}) \times 10^6$ (obtained from the nitrogen reference standards in Table 2 and Equation 1 in Ref. 30).

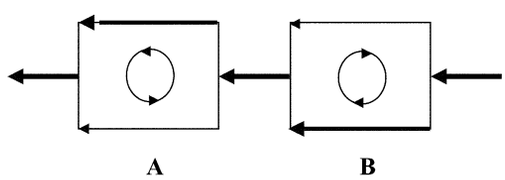

Fig. 3 Schematic representation of bifurcated current flow in a network in which rings exhibit apparent net counterclockwise (A) and clockwise (B) circulations.

Shieldings obtained with the CTOCD-PZ2 formulation, even with the modest 6-31G** basis, have been found to be in remarkably good agreement with experiment for proton and carbon shieldings, particularly the latter.[27,31,32] In the present case, there is fair agreement between experimental and computed values for the deshielding of both peripheral and bridge protons, and the computed value ($\delta = -1.69$) for the internal protons is consistent with the strong shielding expected from the global diamagnetic response to the external field, and also with the broad signal at $\delta = 3.2$ observed in the ^{1}H-NMR spectrum. Assignment of the five signals observed in the ^{13}C-NMR spectrum is more convincing because of the close matching of relative values of the computed and experimental shifts, and even the quaternary carbons pairs (1, 8) and (4, 5) are unambiguously assigned. Most surprising, and gratifying, is the agreement of the computed nitrogen shieldings with the ^{15}N-NMR spectrum.[28] The separate chemical shifts for the imino nitrogen (computed $\delta_{NH} = 113$) and the azomethine nitrogen (computed $\delta_N = 204$) are not observed in porphycene even at low temperature, but the average (159) of the computed values is close to the observed value (161). Furthermore, the individual shifts match closely the corresponding shifts (107 and 215) observed for porphin itself at low temperature,[28] providing some confidence in the present method of computing magnetic properties, and in the underlying current density maps.

References

1 E. Vogel, M. Köcher, H. Schmickler and J. Lex, *Ang. Chem., Int. Ed. Engl.*, 1986, **25**, 257–259.

2 E. Vogel, M. Bröring, J. Fink, D. Rosen, H. Schmickler, J. Lex, K. W. K. Chan, Y.-D. Wu, D. A. Plattner, M. Nendel and K. N. Houk, *Angew. Chem., Int. Ed. Engl.*, 1995, **34**, 2511–2514.
3 O. Arad, A. Gavalda, O. Rey, N. Rubio, D. Sanchez-Garcia, J. I. Borrell, J. Teixido, S. Nonell, M. Canete, A. Juarranz, A. Villanueva, J. C. Stockert and P. J. D. Jimenez, *Afinidad*, 2002, **59**, 343–356.
4 T. Hayashi, H. Dejima, T. Matsuo, H. Sato, D. Murata and Y. Hisaeda, *J. Am. Chem. Soc.*, 2002, **124**, 11226–11227.
5 M. Gouterman, *J. Chem. Phys.*, 1959, **30**, 1139–1161.
6 E. Steiner and P. W. Fowler, *J. Phys. Chem. A*, 2001, **105**, 9553–9562.
7 E. Steiner and P. W. Fowler, *Chem. Commun.*, 2001, 2220–2221.
8 E. Steiner and P. W. Fowler, *ChemPhysChem.*, 2002, **3**, 114–116.
9 E. Steiner and P. W. Fowler, in *Biochemistry and biophysics of chlorophylls*, ed. B. Grimm, R. Porra, W. Rüdiger and H. Scheer, Advances in Photosynthesis, Kluwer, Dordrecht, in press.
10 P. von R. Schleyer, C. Maerker, A. Dransfeld, H. Jiao and N. J. R. van Eikema Hommes, *J. Am. Chem. Soc.*, 1996, **118**, 6317–6318.
11 M. K. Cyrañski, M. Krygowski, M. Wisiorowski, N. J. R. van Eikema Hommes and P. von R. Schleyer, *Angew. Chem., Int. Ed.*, 1998, **37**, 177–180.
12 C. Ochsenfeld, S. P. Brown, I. Schnell, J. Gauss and H. W. Spiess, *J. Am. Chem. Soc.*, 2001, **123**, 2597–2606.
13 Gaussian 98, Revision A.6 M. J. Frisch, G. W. Trucks, H. B. Schlegel, G. E. Scuseria, M. A. Robb, J. R. Cheeseman, V. G. Zakrzewski, J. A. Montgomery, Jr., R. E. Stratmann, J. C. Burant, S. Dapprich, J. M. Millam, A. D. Daniels, K. N. Kudin, M. C. Strain, O. Farkas, J. Tomasi, V. Barone, M. Cossi, R. Cammi, B. Mennucci, C. Pomelli, C. Adamo, S. Clifford, J. Ochterski, G. A. Petersson, P. Y. Ayala, Q. Cui, K. Morokuma, K. Malick, A. D. Rabuck, K. Raghavachari, J. B. Foresman, J. Cioslowski, J. V. Ortiz, B. B. Stefanov, G. Liu, A. Liashenko, P. Piskorz, I. Komaromi, R. Gomperts, R. L. Martin, D. J. Fox, T. Keith, M. A. Al-Laham, C. Y. Peng, A. Nanayakkara, C. Gonzalez, M. Challacombe, P. M. W. Gill, B. Johnson, W. Chen, M. W. Wong, J. L. Andres, C. Gonzalez, M. Head-Gordon, E. S. Replogle, J. A. Pople, Gaussian, Inc., Pittsburgh PA, 1998.
14 P. M. Kozlowski, M. Z. Zgierski and J. Baker, *J. Chem. Phys.*, 1998, **109**, 5905–5913.
15 J. Baker, P. M. Kozlowski, A. A. Jarzecki and P. Pulay, *Theor. Chem. Acc.*, 1997, **97**, 59–66.
16 P. Lazzeretti and R. Zanasi, SYSMO Package; University of Modena: Modena, Italy, 1980; with additional routines for evaluation and plotting of current density by E. Steiner and P. W. Fowler.
17 T. Keith and R. F. W. Bader, *Chem. Phys. Lett.*, 1993, **210**, 223–231.
18 S. Coriani, P. Lazzeretti, M. Malagoli and R. Zanasi, *Theor. Chim. Acta*, 1994, **89**, 181–192.
19 E. Steiner and P. W. Fowler, *Int. J. Quantum Chem.*, 1996, **60**, 609–616.
20 R. Zanasi, P. Lazzeretti, M. Malagoli and F. Piccinini, *J. Chem. Phys.*, 1995, **102**, 7150–7157.
21 T. A. Keith and R. F. W. Bader, *J. Chem. Phys.*, 1993, **99**, 3669–3682.
22 A. Ligabue, A. Soncini and P. Lazzeretti, *J. Am. Chem. Soc.*, 2002, **124**, 2008–2014.
23 I. Cernušák, P. W. Fowler and E. Steiner, *Mol. Phys.*, 1997, **91**, 401–412.
24 J. Jusélius and D. Sundholm, *Phys. Chem. Chem. Phys.*, 2000, **2**, 2145–2151.
25 H. Jiao and P. von R. Schleyer, *J. Phys. Org. Chem.*, 1998, **11**, 655–662.
26 P. von R. Schleyer, M. Manoharan, Z.-X. Wang, B. Kiran, H. Jiao, R. Puchta and N. J. R. van Eikema Hommes, *Org. Lett.*, 2001, **3**, 2465.
27 E. Steiner, P. W. Fowler and L. W. Jenneskens, *Angew. Chem., Int. Ed.*, 2001, **40**, 362–366.
28 B. Wehrle, H.-H. Limbach, M. Köcher, O. Ermer and E. Vogel, *Angew. Chem., Int. Ed. Engl.*, 1987, **26**, 934–936.
29 R. Zanasi, *J. Chem. Phys.*, 1996, **105**, 1460–1469.
30 J. Mason, in *Encyclopedia of Nuclear Magnetic Resonance*, ed. D. M. Grand and R. K. Harris, John Wiley and Sons, Chichester, 1996, vol 5, pp. 3222–3251.
31 P. W. Fowler, E. Steiner, R. Zanasi and B. Cadioli, *Mol. Phys.*, 1999, **96**, 1099–1108.
32 P. W. Fowler, E. Steiner, A. Acocella, L. W. Jenneskens and R. W. A. Havenith, *J. Chem. Soc., Perkin Trans. 2*, 2001, 1058–1065.